Simulation of the nuclear shell-model with quantum circuits.

Author: Carlos Ramon Escandell
*Facultat de Física, Universitat de Barcelona, Diagonal 645, 08028 Barcelona, Spain.**

Advisors: Axel Pérez-Obiol & Bruno Juliá Díaz
Barcelona Supercomputing Center, 08034 Barcelona, Spain† and
Institut de Ciències del Cosmos (ICCUB), c. Martí i Franqués, 1, 08028 Barcelona, Spain‡

Abstract: This thesis focuses on the study of the nuclear shell-model through the implementation of quantum circuits. Each single-particle state in a shell is associated with a qubit in state $|1\rangle$ if occupied and $|0\rangle$ if empty. By employing the system's Hamiltonian and utilizing the Jordan-Wigner mapping, creation and annihilation fermion operators are transformed into Pauli matrix terms, enabling their implementation in a quantum circuit through quantum gates. To simulate this system, an Adaptive Variational Quantum Eigensolver (ADAPT-VQE) is employed, which iteratively constructs a wavefunction that minimizes the energy at each step. Through repeated iterations, an upper bound for the ground state energy is obtained.

I. INTRODUCTION

In the field of nuclear physics, the nuclear shell-model has stood as a cornerstone for the understanding of the nuclear structure. This model has provided deep insights into the behavior of atomic nuclei, yet it faces significant limitations due to the exponential scaling on the basis size as the number of particles increases. One of the most promising approaches to overcoming this challenge is the use of quantum computing [1]. This work aims to explore the potential of quantum circuits for simulating the nuclear shell-model.

The advent of quantum computing has given rise to a new paradigm in computation, which is particularly suited to tackling problems in the field of quantum many body that are intractable for classical computers. Utilizing the principles of quantum superposition and entanglement, quantum computing offers the potential to handle many-body systems that scale exponentially with traditional computing resources. The research presented in this work leverages these quantum capabilities to simulate the nuclear shell-model.

In this study, we will replicate the quantum circuit design strategy from [2] with the intention of reproducing the same results and supplementing them with a study of the measurement. This strategy utilizes an adaptive variational quantum eigensolver (ADAPT-VQE) algorithm, a powerful tool in the current noisy intermediate-scale quantum (NISQ) era [3]. The strength of this approach lies in its hybrid quantum-classical nature, optimizing parameters classically while computing expectation values through quantum measurements [4].

This work is structured as follows: Section II lays the foundation by introducing the fundamentals of the Nuclear shell-model and establishing the motivation for employing quantum computing. Section III elucidates the algorithm employed to solve the Nuclear shell-model and the circuit design strategy implemented for its simulation. The following section, Section IV, will present and dissect our results. Finally, we conclude and summarize in Section V.

II. NUCLEAR SHELL-MODEL

The nuclear shell-model is a fundamental tool in nuclear physics that provides a detailed understanding of the arrangement of nucleons within the nucleus of an atom. This model proposes that the nucleons, which include protons and neutrons, are situated at discrete energy levels inside the atomic nucleus. Notably, experimental observations revealed the existence of certain "magic numbers" of nucleons that demonstrated peculiar characteristics. These "magic numbers" (N or Z = 2, 8, 20, 28, 50, 82, 126, 184) were associated with an unexpectedly high binding energy, a smaller nuclear radius, a reduction in the neutron capture cross-section, and an increased energy of alpha particles when the remaining nucleus was characterized as "magic".

According to the principles of the nuclear shell-model, the atomic nucleus can be conceptualized as being constituted of two distinct parts. The first part is an inert core, which consists of nucleons that have reached a "magic number". These nucleons are dynamically paired and they don't actively participate in the system's dynamics. The second part, consists of the remaining neutrons and protons that do not complete a magic number. These particles are located in what is known as the "valence space". It is within relatively limited valence space that these neutrons and protons interact and significantly contribute to the properties of the nucleus [5].
With this description, we can formulate an effective Hamiltonian for this valence space, which can be expressed as: [2]

$$H_{\text{eff}} = \sum_i \epsilon_i a_i^\dagger a_i + \frac{1}{4} \sum_{ijkl} \bar{v}_{ijkl} a_i^\dagger a_j^\dagger a_l a_k. \qquad (1)$$

*Electronic address: cramones10@alumnes.ub.edu
†Electronic address: axel.perezobiol@bsc.es
‡Electronic address: brunojulia@ub.edu

Here, ϵ_i is the single-particle energy of state i, while $\bar{v}_{ijkl} = v_{ijkl} - v_{ijlk}$ refers to the the two-body antisymmetric phenomenological couplings. Additionally, a_i and $a_i^\dagger$ are the annihilation and creation operators, respectively.

Since the nuclear force is rotationally invariant and nucleons are fermions, a single-particle basis with quantum numbers nl_j will be used, with n as the principal quantum number, l the orbital angular momentum, and j the total angular momentum. This basis also includes the third component m of the projections of j. To distinguish between protons and neutrons, the isospin quantum number $t = 1/2$ with its third component $t_z = \pm 1/2$, $+$ for protons and $-$ for neutrons, is included in the basis. With these considerations, a suitable basis is the M-scheme, where the Slater determinant is chosen such that it has a well-defined M. The nuclear states can be expanded in this basis as follows:

$$|JM\ TT_z\rangle = \sum_\alpha c_\alpha |\alpha, MT_z\rangle, \tag{2}$$

where $\alpha = n_\alpha l_\alpha j_\alpha t_\alpha$ [6]. A challenge with this system is that the number of Slater determinants grows according to:

$$dim_{mb} = \binom{dim_{sp}}{N_{CI}} \times \binom{dim_{sp}}{Z_{CI}}. \tag{3}$$

Here, N_{CI} and Z_{CI} are the numbers of active neutrons and protons in the configuration space, respectively, and dim_{sp} is the dimension of the single-particle basis of a nuclear shell consisting of different nl_j orbitals, thus defined as $dim_{sp} = \sum_j (2j+1)$. This sum provides the total number of states in the shell, which is the dimension of the single-particle basis within that shell [2].

In summary, the nuclear shell-model offers a comprehensive approach to understanding the structure and behavior of atomic nuclei. However, the model faces challenges, especially when dealing with heavier nuclei with a large number of nucleons. The dimension of the many-body Hilbert space, scales exponentially with the number of particles making classical simulations of the model increasingly difficult. This is where quantum computing comes into the picture.

In light of this, the following discussion will delve into the exciting potential of the ADAPT-VQE algorithm to address the complexities of the nuclear shell-model.

III. VARIATIONAL ALGORITHM AND QUANTUM CIRCUIT DESIGN STRATEGY.

Firstly, the variational algorithm used to simulate the nuclear shell-model will be presented, followed by a discussion on the strategy implemented to construct the corresponding quantum circuit.

A. ADAPT-VQE

The variational algorithm employed in our study of the nuclear shell-model is an ADAPT-VQE. This algorithm iteratively constructs a wavefunction of the form:

$$|\Psi(\boldsymbol{\theta})\rangle = \prod_{k=1}^{n} e^{i\theta_k A_k} |\text{ref}\rangle, \tag{4}$$

here, $\boldsymbol{\theta} = \{\theta_k,\ k = 1, \ldots, n\}$ denotes a set of variational parameters, where an additional parameter is introduced in each iteration, A_k are combinations of creation and annihilation fermion operators, and $|\text{ref}\rangle$ is the reference state upon which we iterate. What this algorithm does is to select the set of variational parameters $\boldsymbol{\theta}$ that minimize the energy according to:

$$E_{\text{ADAPT-VQE}} = \min_{\boldsymbol{\theta}} \frac{\langle\psi(\boldsymbol{\theta})|H_{\text{eff}}|\psi(\boldsymbol{\theta})\rangle}{\langle\psi(\boldsymbol{\theta})|\psi(\boldsymbol{\theta})\rangle}. \tag{5}$$

Subsequently, the ansatz is evolved according to a unitarian transformation $|\Psi(\boldsymbol{\theta})\rangle \to e^{i\theta_k A_k}|\Psi(\boldsymbol{\theta})\rangle$ where the new operator A_k is obtained based on the operator that yields the largest gradient:

$$\left.\frac{\partial E^{(n)}}{\partial \theta_k}\right|_{\theta_k=0} = i\,\langle\psi(\boldsymbol{\theta})|[H_{\text{eff}}, A_k]|\psi(\boldsymbol{\theta})\rangle\,|_{\theta_k=0}. \tag{6}$$

All available operators A_k are predefined before beginning the simulation. Given that we are working with the nuclear shell-model, these operators must conserve the number of particles, total angular momentum J, its z-projection M, parity Π, and the third component of isospin T_z. This motivates us to use the following two-body fermionic operators:

$$T^{pq}_{rs} = i(a_p^\dagger a_q^\dagger a_r a_s - a_r^\dagger a_s^\dagger a_p a_q), \tag{7}$$

where p, q, r, and s are single-particle states with their quantum numbers n, l, j, m, and t_z.

On the other hand, another preparatory operation before starting the simulation is to determine the state $|\text{ref}\rangle$ from which the iteration begins. This state is chosen as the member of the Fock basis that exhibits a lower energy configuration within the Hamiltonian. This strategic choice aims to reduce the number of iterations required by the algorithm.

Therefore, the ADAPT-VQE algorithm implements the following steps:

1. Calculate all non-zero operators T^{pq}_{rs} in the basis of the valence space to be worked on.
2. Determine the Fock state of minimum energy of the Hamiltonian from which the VQE iteration will begin.
3. Given this state, find the operator T^{pq}_{rs} that gives us the maximum gradient.
4. Find the values of $\boldsymbol{\theta}$ that gives the smallest energy value using a classical optimizer, in this case, we have employed the (gradient based) BFGS optimizer.
5. Evolve our state from $|\Psi(\boldsymbol{\theta})\rangle$ to $e^{i\theta_k A_k}|\Psi(\boldsymbol{\theta})\rangle$.
6. Return to the third step and iterate until the system converges to the Ground State.

B. QUANTUM CIRCUIT DESIGN STRATEGY

In this subsection, we outline the steps to build the circuit for the variational algorithm. We begin with the Mapping (III B 1), transforming the fermionic operators T^{pq}_{rs} and the effective Hamiltonian of the valence space into Pauli matrices via the Jordan-Wigner transformation. Subsequently, we prepare the initial state in the quantum circuit (III B 2) as previously detailed. Following this, we carry out the variational optimization (III B 3), elaborating the circuit that evolves the state $|\psi(\boldsymbol{\theta})\rangle \to e^{i\theta_k A_k}|\psi(\boldsymbol{\theta})\rangle$. And ultimately, we measure the expected value of the Hamiltonian to compute the energy (III B 4).

1. Mapping

The transformation of fermionic annihilation and creation operators into Pauli strings is a key step [7]. This transformation is achieved through the Jordan-Wigner transformation, where the operators are transformed as follows:

$$a_i^\dagger = \left(\prod_{k=0}^{i-1} Z_k\right)\sigma_i^-, \qquad a_i = \left(\prod_{k=0}^{i-1} Z_k\right)\sigma_i^+. \tag{8}$$

Here, $\sigma_j^\pm = \frac{1}{2}(X_j \pm iY_j)$ where j represents the specific qubit upon which the operator acts.

Subsequently, the fermionic operators T^{pq}_{rs} are converted to Pauli strings. In this case, the operator transformation is represented by the equations (13) and (14) elaborated in the Appendix.

Moreover, the Hamiltonian (1) contains one-body operators $n_p = a_p^\dagger a_p$ and two-body operators $h_{pqrs} = a_p^\dagger a_q^\dagger a_r a_s + a_r^\dagger a_s^\dagger a_p a_q$. The respective Jordan-Wigner transformations of these operators are also detailed in the Appendix (Equations (15) and (16), respectively).

2. Initial state preparation

The initial state to begin the iteration, $|\text{ref}\rangle$, is the Fock's state of lowest energy of the Hamiltonian. This state can be efficiently obtained through a classical search that requires at most dim_{mb} operations. Once the state has been determined, the circuit is modified with X gates, bearing in mind that it always starts with all qubits in the $|0\rangle$ state. For example, when considering the Beryllium-10 isotope, which has 4 neutrons and 2 protons in the valence shell, we find that this state corresponds to:

$$|\psi_0\rangle = a_1^\dagger a_2^\dagger a_6^\dagger a_7^\dagger a_8^\dagger a_9^\dagger|\text{vac}\rangle. \tag{9}$$

Where $|\text{vac}\rangle$ corresponds to the valence shell with no fermions (vacuum). This state can also be written as:

$$|\psi_0\rangle = |0110001111000\rangle = X_1X_2X_6X_7X_8X_9|0\rangle^{\otimes 12}. \tag{10}$$

Hence, to obtain this state in the quantum circuit, it will suffice to apply an X gate on qubits 1, 2, 6, 7, 8, and 9.

3. Variational optimization

In the initial iteration of the algorithm, we will find the operator T^{pq}_{rs} with largest gradient from a previously computed pool of operators according to equation (6). Having obtained the first T^{pq}_{rs}, we need to evolve the initial state $|\psi_0\rangle \to e^{iT^{pq}_{rs}\theta_0}|\psi_0\rangle$ and compute the θ_0 that minimizes the energy value. Afterwards, the algorithm consists of iterating this process by adding a new θ parameter each time and optimizing all of them simultaneously in each energy calculation, until the ground state energy is reached.

Each T^{pq}_{rs} consists solely of Pauli strings that commute with each other due to the exclusive presence of X and Y and an even number of variations between them. Consequently, each T^{pq}_{rs} can be exponentiated individually, eliminating the need for the Trotter-Suzuki approximation.

To construct the quantum circuit that performs the evolution $e^{iT^{pq}_{rs}\theta_k}$, we employ the Staircase Algorithm [8]. This algorithm is structured such that if the Pauli Strings contain only Z gates, the circuit will have two cascades of CNOTs and one $R_z(\theta) = e^{-i\frac{\theta}{2}Z}$ rotation. Given that the Jordan-Wigner transformation yields both X and Y gates, we will implement a basis change of the form $X = HZH$ and $Y = R_x^\dagger Z R_x$. Thus, in the circuit, we will first have H and $R_x^\dagger$ rotations, followed by the first cascade of CNOTs, the $R_z(\theta)$ rotation on the last qubit, the next cascade of CNOTs, and finally the H and R_x gates to reverse the basis change [9].

Let's examine an example for a case involving 4 qubits. Suppose we have a core layer with 4 qubits, with an initial state $|\psi_0\rangle = X_0X_2|\text{ref}\rangle$, and we aim to implement the circuit $e^{-i\frac{\theta}{2}X_0Y_1Z_2Z_3}$. The resulting circuit would be:

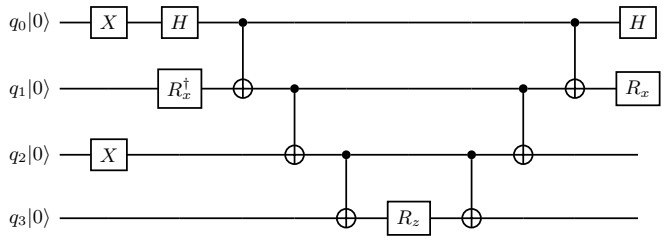

FIG. 1: This circuit implements the state $|\psi\rangle = e^{-i\frac{\theta}{2}X_0Y_1Z_2Z_3}X_0X_2|0\rangle^{\otimes 4}$ through the staircase algorithm.

4. Measurement

Up to this point, we have the circuit that evolves $|\psi(\boldsymbol{\theta})\rangle$. Our goal now is to compute the expectation value $\langle\psi(\boldsymbol{\theta})|H_{\text{eff}}|\psi(\boldsymbol{\theta})\rangle$. Therefore, the strategy we have adopted involves decomposing the Hamiltonian (1) into four distinct terms. On the one hand, we have single-body operators n_i which, upon carrying out the Jordan-Wigner transformation, become diagonal and can thus be measured directly: $\langle\psi_n|n_i|\psi_n\rangle = \frac{1}{2}\langle\psi_n|1 - Z_i|\psi_n\rangle = p_1^{(i)}$ where $p_1^{(i)}$ is the probability of measuring 1 in the i-th qubit.

On the other hand, we have the two-body terms of

the Hamiltonian. These can be categorized into three types based on their indices. The first, h_{ijij} (and its indices permutations), simply represents the product of two single-body operators. This relationship can be expressed as $\langle\psi_n|h_{ijij}|\psi_n\rangle = -2\langle\psi_n|n_i n_j|\psi_n\rangle = -2p_{11}^{(ij)}$, where $p_{11}^{(ij)}$ denotes the probability of measuring 1 in qubits i and j. The second type, h_{ijik}, can be diagonalized through a basis change employing $M_{jk} = CX_{kj}H_kCX_{kj}$, where CX_{ij} represents the CNOT gate acting on qubits i and j. Once diagonalized, assuming contiguous indices, the expectation value is given by $\langle\psi_n|h_{ijik}|\psi_n\rangle = p_{101}^{(ijk)} - p_{110}^{(ijk)}$. Lastly, h_{ijkl}, similar to the second type, can be diagonalized using the basis change $M_{ijkl} = CX_{ij}CX_{ki}CX_{lk}H_lCX_{lk}CX_{ki}CX_{ij}$. The expectation value for this type can be represented as $\langle\psi_n|h_{ijkl}|\psi_n\rangle = p_{1100}^{(ijkl)} - p_{0011}^{(ijkl)}$, where $p_{r_1\dots r_k}^{q_1\cdots q_k}$ are the probabilities of measuring $r_1\dots r_k$ in the qubits $q_1\dots q_k$ on the vector over which the basis change has been made [2].

IV. SIMULATION

In this section, we present the ADAPT-VQE simulation results for Lithium-6, Beryllium-10, and Oxygen-18. As the results are probabilistic, their precision increases with the number of measurements. Specifically, we analyze the standard deviation of expected value calculations of one-body and two-body operators for Oxygen-18, a study that could be extended to the other Hamiltonian terms and nuclei.

We compare the energy values computed classically (through Hamiltonian diagonalization) to those determined by our variational algorithm, highlighting that our computed energy, as in all variational methods, provides an upper bound to the ground state energy. Further, we graph the relative error, $\epsilon_E = \frac{|E_{\text{ADAPT-VQE}} - E|}{E}$, over iterations, demonstrating the precision of our approximation. The code for these simulations can be found in the repository [10].

A. Lithium-6

Lithium-6 is constituted of 3 neutrons (N=3) and 3 protons (Z=3), consequently, we have 1 neutron and 1 proton in the valence shell, situating us within the p-shell and requiring 12 qubits for a quantum simulation. The algorithm finds itself stagnated in a local minimum when initiating in the Fock's basis minimum energy state, $|\psi_0\rangle = a_2^\dagger a_7^\dagger|\text{vac}\rangle$. To address this issue, we initiate the system in an alternate state of the basis: $|\psi_0\rangle = a_1^\dagger a_{11}^\dagger|\text{vac}\rangle$. The results obtained for this nucleus can be observed on the left panels of Figure 3.

The derived wave function is:

$$|\psi_{^6\text{Li}}\rangle = e^{i\theta_8 T_{5,7}^{1,11}} e^{i\theta_7 T_{0,9}^{5,7}} e^{i\theta_6 T_{3,6}^{5,7}} e^{i\theta_5 T_{2,10}^{1,11}} e^{i\theta_4 T_{5,7}^{4,8}} e^{i\theta_3 T_{5,10}^{3,6}} e^{i\theta_2 T_{4,11}^{3,6}} e^{i\theta_1 T_{5,7}^{1,8}} e^{i\theta_0 T_{2,7}^{0,9}} X_1 X_{11}|0\rangle^{\otimes 12}.$$

Where: $\theta_0 = -0.95175$, $\theta_1 = -0.5120$, $\theta_2 = -0.58015$, $\theta_3 = 0.78540$, $\theta_4 = -0.76281$, $\theta_5 = -0.16489$, $\theta_6 = -0.16718$, $\theta_7 = 0.29835$ and $\theta_8 = 0.32175$.

B. Beryllium-10

Beryllium-10 is composed of 6 neutrons ($N = 6$) and 4 protons ($Z = 4$). As a result, there are 4 neutrons and 2 protons in the valence shell, requiring a total of 12 qubits for simulation within the p-shell. The Fock state of the basis, characterized by the minimum energy, is represented in equation (9). From this starting state, we obtain the results depicted in the central plot of Figure 3. A total of 48 iterations were necessary to achieve the ground state energy with a relative error of $\epsilon_E \approx 10^{-5}$.

C. Oxygen-18

Oxygen-18, with 10 neutrons ($N = 10$) and 8 protons ($Z = 8$), has 2 neutrons in the valence sd-shell, requiring 12 qubits for simulation. Starting from the state $|\psi_0\rangle = a_0^\dagger a_5^\dagger|\text{vac}\rangle$, the simulation results are displayed on the right panel of Figure 3. The wave function derived is given by:

$$|\psi_{^{18}\text{O}}\rangle = e^{i\theta_4 T_{2,3}^{0,5}} e^{i\theta_3 T_{9,10}^{0,5}} e^{i\theta_2 T_{1,4}^{0,5}} e^{i\theta_1 T_{6,7}^{0,5}} e^{i\theta_0 T_{8,11}^{0,5}} X_0 X_5|0\rangle^{\otimes 12}.$$

With parameters: $\theta_0 = -0.15726$, $\theta_1 = -0.43724$, $\theta_2 = 0.60466$, $\theta_3 = 0.21443$, $\theta_4 = -0.78547$.

By calculating the expected value of the operators n_i and h_{ijij}, we find that the standard deviation decreases with $\sigma = \frac{c}{\sqrt{N}}$, where N represents the number of circuit measurements, with $c_{n_i} = 5.97\times10^{-1}$ and $c_{h_{ijij}} = 7,62\times 10^{-2}$.

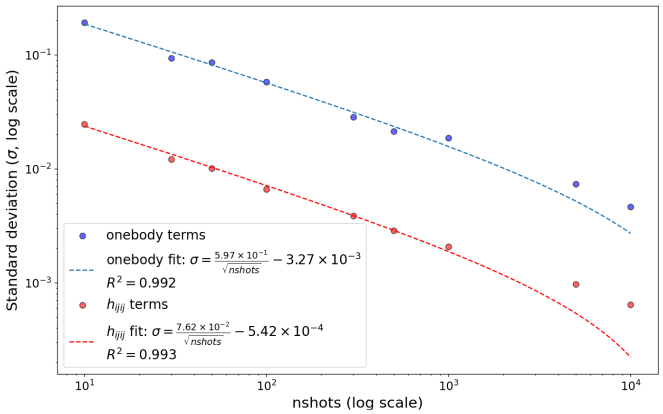

FIG. 2: Double-logarithmic plot depicting the standard deviation dependency on the number of repetitions for the calculation of the expected values of $\langle n_i\rangle$ and $\langle h_{ijij}\rangle$.

V. CONCLUSION

In this study, we have explored an alternative to the traditional method of simulating the ground state of various nuclei using classical diagonalization of the Hamiltonian. The theoretical model employed for describing the physics of nuclei is the nuclear shell-model. However, this model presents a challenge when attempting to simulate it with a classical computer due to its rapid scaling with the number of particles.

One of the main advantages that quantum computing offers in this context is that it requires only as many

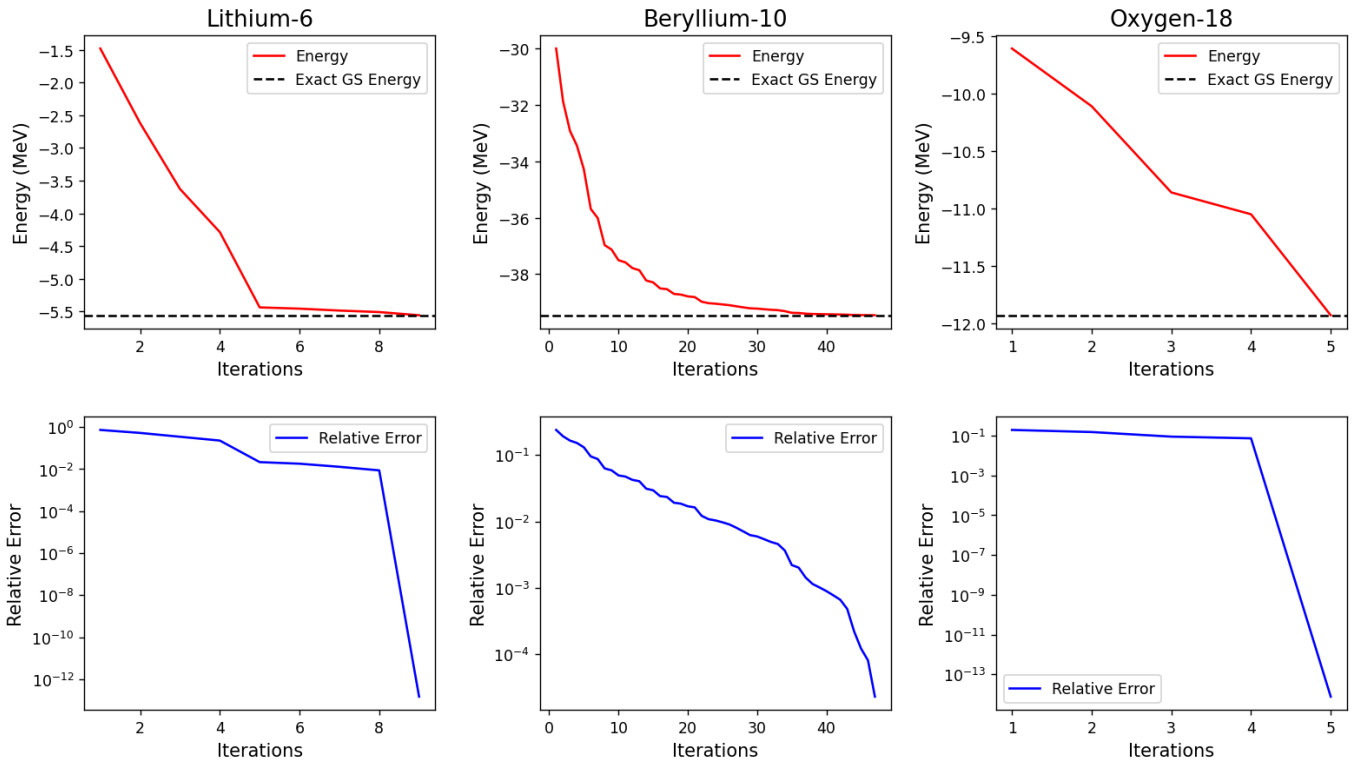

FIG. 3: In the upper part of the multiplot, shown in red, we have plotted how the energy converges towards the value of its ground state energy as a function of the number of iterations. In the lower part, shown in blue, we have plotted the relative error as more iterations are performed. The graphics on the left correspond to Lithium-6, the central graphics to Beryllium-10, and those on the right to Oxygen-18.

qubits as there are possible states in the valence shell to simulate the presented algorithm. Importantly, this extends to both memory and computational time resources, demonstrating a significant departure from classical computing practices and provides a path to overcome computational barriers in nuclear physics simulations. Nevertheless, a critical area for future investigation is the examination of how circuit depth scales for heavier nuclei.

The algorithm was successfully executed, enabling us to determine the ground state energy of three distinct nuclei: Oxygen-18, Beryllium-10, and Lithium-6. This accomplishment affirms the potential viability of quantum approaches to nuclear shell-model simulations. The accuracy demonstrated is comparable to classical methods, yet promises enhanced scalability for larger systems.

Acknowledgments

I would like to thank Dr. Axel Pérez-Obiol for granting me the opportunity to learn from him through our numerous discussions and for the invaluable experience of being part of the quantic group at the BSC. His guidance, patience and insightful feedback have been instrumental in the successful completion of this work.

[1] A. M. Romero et al. “Solving nuclear structure problems with the adaptive variational quantum algorithm”, Physical Review C, vol. 105, no. 6, 2022.
[2] A. Pérez-Obiol et al. “Nuclear shell-model simulation in digital quantum computers”, arXiv preprint arXiv:2302.03641, 2023.
[3] M. Cerezo et al. “Variational quantum algorithms”, Nature Reviews Physics, vol. 3, no. 9, pp. 625-644, 2021.
[4] A. Peruzzo et al., “A variational eigenvalue solver on a photonic quantum processor”, Nature Communications, vol. 5, no. 1, 2014.
[5] Kenneth S. Krane, *Introductory Nuclear Physics*, (John Wiley & Sons, New York, NY, 1987) : p. 116-156.
[6] Jouni Suhonen, *From Nucleons to Nucleus: Concepts of Microscopic Nuclear Theory*, (Springer Berlin Heidelberg New York, Berlin, Heidelberg, New York, 2007) :p. 39-60.
[7] P. Jordan and E. P. Wigner, “The Collected Works of Eugene Paul Wigner”, pp. 109-129, Springer, 1993.
[8] Yordan S. Yordanov et al “Efficient quantum circuits for quantum computational chemistry”, Physical Review A, vol. 102, no. 6, 2020.
[9] Maximilian Balthasar Mansky et al. “Decomposition Algorithm of an Arbitrary Pauli Exponential through a Quantum Circuit”, arXiv:2305.04807, 2023.
[10] Carlos Ramon, *Final Degree Project*, GitHub repository, (2023), Available: `https://github.com/apeyron0/TFG-Carlos-Ramon`

VI. Appendix

A. Deduction of the equation that gives the maximum gradient operator

We will demonstrate the following equation:

$$\left.\frac{\partial E^{(n)}}{\partial \theta_k}\right|_{\theta_k=0} = i\,\langle\psi(\boldsymbol{\theta})|[H_{\text{eff}}, A_k]|\psi(\boldsymbol{\theta})\rangle\,|_{\theta_k=0}.$$

We begin with the expression for the minimization of energy:

$$E_{\text{ADAPT-VQE}} = \min_{\theta} \frac{\langle\psi(\boldsymbol{\theta})|H_{\text{eff}}|\psi(\boldsymbol{\theta})\rangle}{\langle\psi(\boldsymbol{\theta})|\psi(\boldsymbol{\theta})\rangle}.$$

Since the wave function is already normalized, we can write the energy as $E = \langle\psi(\boldsymbol{\theta})|H_{\text{eff}}|\psi(\boldsymbol{\theta})\rangle$. At each step k of the iterative procedure, the ansatz is expanded by: $|\psi(\theta\rangle \rightarrow e^{i\theta_k A_k}|\psi(\theta\rangle$. Therefore, at each step, we need to compute:

$$E = \langle e^{i\theta_k A_k}\psi(\boldsymbol{\theta})|H_{\text{eff}}|e^{i\theta_k A_k}\psi(\boldsymbol{\theta})\rangle.$$

Differentiating this expression with respect to θ_k yields:

$$\begin{aligned}\frac{\partial E}{\partial \theta_k} &= \frac{\partial}{\partial \theta_k}\left\langle e^{i\theta_k A_k}\psi(\boldsymbol{\theta})|H_{\text{eff}}|e^{i\theta_k A_k}\psi(\boldsymbol{\theta})\right\rangle \\ &= \left\langle \psi(\boldsymbol{\theta})\left|\frac{\partial}{\partial \theta_k}[e^{-i\theta_k A_k}\ H_{\text{eff}}\ e^{i\theta_k A_k}]\right|\psi(\boldsymbol{\theta})\right\rangle\end{aligned}$$

$$\begin{aligned}&= \langle\psi(\boldsymbol{\theta})\,|e^{-i\theta_k A_k}\,(-iA_k)\ H_{\text{eff}}\,e^{i\theta_k A_k} \\ &\qquad +e^{-i\theta_k A_k}\ H_{\text{eff}}\ (iA_k)e^{i\theta_k A_k}\,|\,\psi(\boldsymbol{\theta})\rangle\end{aligned}$$

$$\begin{aligned}&= i\left\langle\psi(\boldsymbol{\theta})\,|e^{-i\theta_k A_k}\,[-A_k\ H_{\text{eff}}\ +\ H_{\text{eff}}\ A_k]\,e^{i\theta_k A_k}\,|\,\psi(\boldsymbol{\theta})\right\rangle \\ &= i\left\langle e^{i\theta_k A_k}\psi(\boldsymbol{\theta})|[H_{\text{eff}}, A_k]|e^{i\theta_k A_k}\psi(\boldsymbol{\theta})\right\rangle.\end{aligned}$$

To derive the final result, we evaluate this expression at $\theta_k = 0$ to obtain:

$$\left.\frac{\partial E}{\partial \theta_k}\right|_{\theta_k=0} = i\,\langle\psi(\boldsymbol{\theta})|[H_{\text{eff}}, A_k]|\psi(\boldsymbol{\theta})\rangle\,|_{\theta_k=0}. \tag{11}$$

In conclusion, we have shown that the derivative of the energy with respect to the parameter θ_k is equal to the commutator of the Hamiltonian and the operator A_k, evaluated at $\theta_k = 0$.
We note that we have not studied the measurement protocol for these terms and in our simulations we have computed this expression analytically.

In the case we are dealing with, where the matrices H_{eff} and A_k are very large, it is useful to simplify the commutator and reduce it to a single matrix product. To achieve this, we assume that both H_{eff} and A_k are Hermitian and attempt to simplify the problem:

$$\begin{aligned}&i\,\langle\psi(\boldsymbol{\theta})|[H_{\text{eff}}, A_k]|\psi(\boldsymbol{\theta})\rangle \\ =&i\,[\langle\psi(\boldsymbol{\theta})|H_{\text{eff}}A_k|\psi(\boldsymbol{\theta})\rangle - \langle\psi(\boldsymbol{\theta})|A_k H_{\text{eff}}|\psi(\boldsymbol{\theta})\rangle] \\ =&i\left[\left\langle|H_{\text{eff}}^{\dagger}\psi(\boldsymbol{\theta})|A_k\psi(\boldsymbol{\theta})\right\rangle - \left\langle A_k^{\dagger}\psi(\boldsymbol{\theta})|H_{\text{eff}}\psi(\boldsymbol{\theta})\right\rangle\right] \\ =&i\,[\langle|H_{\text{eff}}\psi(\boldsymbol{\theta})|A_k\psi(\boldsymbol{\theta})\rangle - \langle A_k\psi(\boldsymbol{\theta})|H_{\text{eff}}\psi(\boldsymbol{\theta})\rangle] \\ =&i\left[\langle|H_{\text{eff}}\psi(\boldsymbol{\theta})|A_k\psi(\boldsymbol{\theta})\rangle - (\langle H_{\text{eff}}\psi(\boldsymbol{\theta})|A_k\psi(\boldsymbol{\theta})\rangle)^*\right].\end{aligned}$$

If we define $z = \langle|H_{\text{eff}}\psi(\boldsymbol{\theta})|A_k\psi(\boldsymbol{\theta})\rangle$:

$$i\,[z - z^*] = i\,[(a+ib) - (a-ib)] = i[2ib] = -2b = -2{\cdot}\text{Im}(z).$$

Thus, we have shown that we can write:

$$i\,\langle\psi(\boldsymbol{\theta})|[H_{\text{eff}}, A_k]|\psi(\boldsymbol{\theta})\rangle = -2\cdot Im\,[\langle\psi(\boldsymbol{\theta})|H_{\text{eff}}A_k|\psi(\boldsymbol{\theta})\rangle] \tag{12}$$

B. Detailed Jordan-Wigner Transformations

Here we present the explicit transformations of the fermionic operators T_{rs}^{pq}, one-body operators n_p, and two-body operators h_{pqrs} to Pauli strings using the Jordan-Wigner transformation.

The fermionic operators T_{rs}^{pq} are transformed as:

$$\begin{aligned}T_{rs}^{pq} &= i(a_p^{\dagger}a_q^{\dagger}a_r a_s - a_r^{\dagger}a_s^{\dagger}a_p a_q) = \\ &\frac{1}{8}P_{rs}^{pq}\,(-X_pX_qY_rY_s - Y_pY_qY_rY_s + Y_pY_qX_rX_s \\ &\quad +Y_pY_qY_rX_s + Y_pX_qX_rX_s + X_pY_qX_rX_s \\ &\quad -X_pX_qY_rX_s - X_pX_qX_rY_s)\,,\end{aligned} \tag{13}$$

where:

$$P_{rs}^{pq} = \left(\prod_{m=p+1,m\notin[r,s]}^{q-1} Z_m\right)\left(\prod_{n=r+1,n\notin[p,q]}^{q-1} Z_n\right). \tag{14}$$

The one-body operator n_p takes the form:

$$n_p = a_p a_p^{\dagger} = \frac{1}{2}(1 - Z_P). \tag{15}$$

Lastly, the transformation of the two-body operator h_{pqrs} is:

$$\begin{aligned}h_{pqrs} &= a_p^{\dagger}a_q^{\dagger}a_r a_s + a_r^{\dagger}a_s^{\dagger}a_p a_q = \\ &\frac{1}{8}P_{rs}^{pq}\,(-X_pX_qX_rX_s + X_pX_qY_rY_s - X_pY_qX_rY_s \\ &\quad -X_pY_qY_rX_s - Y_pY_qY_rY_s + Y_pY_qX_rX_s \\ &\quad -Y_pX_qY_rX_s - Y_pX_qX_rY_s)\,.\end{aligned} \tag{16}$$